arXiv:1612.04696v1 [cond-mat.supr-con] 14 Dec 2016

Transport in Ferromagnet/Superconductor spin valves

Evan Moen[1,*] and Oriol T. Valls[1,†]

[1]*School of Physics and Astronomy, University of Minnesota, Minneapolis, Minnesota 55455*

(Dated: December 15, 2016)

We consider charge transport properties in realistic, fabricable, Ferromagnet/Superconductor spin valves having a layered structure $F_1/N/F_2/S$, where F_1 and F_2 denote the ferromagnets, S the superconductor, and N the normal metal spacer usually inserted in actual devices. Our calculation is fully self-consistent, as required to ensure that conservation laws are satisfied. We include the effects of scattering at all the interfaces. We obtain results for the device conductance G, as a function of bias voltage, for all values of the angle ϕ between the magnetizations of the F_1 and F_2 layers and a range of realistic values for the material and geometrical parameters in the sample. We discuss, in the context of our results for G, the relative influence of all parameters on the spin valve properties. We study also the spin current and the corresponding spin transfer torque in $F_1/F_2/S$ structures.

PACS numbers: 74.45.+c,74.78.Fk,75.75.-c

I. INTRODUCTION

Traditional spin valves[1] consist of two ferromagnetic materials where changing the relative orientation of their exchange fields is used to control the transport properties of the heterostructure. They are based on the well-known and much celebrated[2] Giant Magnetoresistive (GMR) effect. More recently, it has become possible to fabricate spin valves by layering ferromagnetic (F) and superconducting (S) materials. In this context, spintronic devices of various kinds[3–5] have been proposed and considered. The fundamental properties of such devices arise from the F/S proximity effects[6]. These effects lead to many new properties. In particular, spin valve devices, having an $F_1/F_2/S$ or (more typically in experimental situations) $F_1/N/F_2/S$, where N is a normal spacer, have been extensively[7–10] studied both theoretically and experimentally. Research on these devices is furthered because, besides their great scientific interest, they have possible applications towards the creation of non-volatile magnetic memory elements. The supercurrents can also be spin-polarized, and this can then lead to a low energy spin transfer torque that can be used to control the magnetization of nanoscale devices.

Ferromagnetism and s-wave superconductivity would appear to be incompatible due to the opposite spin structure of their order parameters: the internal fields in the ferromagnets tend to break the singlet Cooper pairs. Indeed, although proximity effects do exist in F/S heterostructures, they are very different from those at N/S interfaces. The exchange field leads to the Cooper pairs acquiring a center of mass momentum[11] which results in damped oscillatory behavior of the singlet pair amplitudes in the F layer regions[12–14]. This behavior is fundamentally important: it induces oscillations in most of the physical properties of these structures, including the dependence of the transition temperature[6] on the thickness of the various layers. It also drastically changes the behavior of transport quantities such as the the bias dependent conductance, discussed below.

An even more noteworthy phenomenon arising from the F/S proximity effects is that in certain F/S heterostructures triplet correlations may be induced, even though the S material is an s-wave superconductor[15–17]. These triplet correlations are necessarily odd in frequency[18] or, equivalently, odd in time[16,19] as required by the Pauli principle. When the ferromagnetic exchange fields are all aligned only the $m_z = 0$ triplet component can be induced since S_z, the z component of the Cooper pair spin, commutes with the Hamiltonian. However, when there are two or more F layers with non-collinear exchange fields, as can happen for example in $F_1/F_2/S$ structures, S_z cannot commute with the Hamiltonian and the $m_z = \pm 1$ triplet states can also be induced. This is also the case with a single F layer having a non-uniform magnetization texture[20–23]. In contrast to the short-range proximity-induced singlet pair amplitudes, these odd $m_z = \pm 1$ triplet states are usually long ranged[24–30] in the F layers. Their behavior is also oscillatory. Because of this, the details of the geometry of the F/S multilayers are crucial to determining their equilibrium[31] properties, including the oscillatory behavior of the transition temperature with layer thicknesses and with the misalignment angle ϕ between the two F layers in a spin valve[32]. The transport properties[8] are also affected. As in a conventional spin valve, the relative exchange field orientation of the F layers can have a large effect on the conductance of the system. The introduction of triplet correlations can lead to a nonmonotonic dependence of the conductance on ϕ, just as for equilibrium quantities.

Ultimately, all superconducting proximity effects are governed by Andreev reflection at the interfaces. Andreev reflection[33] is the process of electron-to-hole conversion by the creation or annihilation of a Cooper pair in the superconducting layer. In conventional Andreev reflection, the reflected electron/hole has opposite spin to the incident particle. However, it has been shown[8,34–37] that in F/S interfaces triplet proximity effects are correlated with anomalous Andreev reflection, in which the reflected quasiparticle has the same spin as the incident one. From this, it follows that the transport properties are highly dependent on the proper consideration of Andreev reflection, as has been long recognized in both N/S[38,39] and F/S[40–42] systems. These effects are particularly important when examining the tunneling conductance in the subgap bias regime where such systems can carry a supercurrent.

In this paper, we are motivated by the increasing interest

in building actual, practical spin valve structures with potential use as part of memory elements. We therefore investigate the charge transport properties of a superconducting spin valve, an $F_1/N/F_2/S$ structure which includes the normal metal layer spacer, as used in spin valve devices. This normal metal spacer is necessary in experiments in order to control the relative exchange field of the F layers through the use, for example, of a pinned and a soft ferromagnetic layer, in which the spacer decouples the ferromagnetic layers layers (see e.g. Ref. 32). We will use typical values of the different thicknesses, as in existing and planned devices, and realistic interfacial scattering between the different layers. Parameters such as the exchange field and coherence length will be taken to be in the range relevant to the materials actually used. We are particularly motivated to identify the relevant experimental transport features of actual $F_1/N/F_2/S$ nanoscale systems. Thus, we investigate a geometry corresponding to experimentally realistic nanopillars with a normal metal layer spacer between two ferromagnetic layers. These $F/N/F$ layers are grown on top of a superconducting substrate. This substrate must be thick enough to allow for the sample to be superconducting: its thickness must exceed the superconducting correlation length. Furthermore, experimental constraints do not allow for perfect interfaces. Although recent developments in fabrication techniques[4] have allowed for very clean interfaces with ballistic transport properties, surface imperfections are unavoidable and even small interfacial scattering can have a large effect on the transport properties, as we shall see, since they affect both ordinary and Andreev scattering. We will use a self consistent solution of the Bogoliubov de Gennes (BdG) equations[43] to calculate the conductance G as a function of bias voltage for realistic ranges of geometrical and material parameters, and as a function of the angle ϕ. Temperature corrections, which we will show to be non negligible, will also be studied. The conductance will be obtained from the self consistent solutions of the Hamiltonian, via a transfer matrix procedure which makes use of the Blonder-Tinkham-Klapwijk (BTK) method[38]. In some previous calculations[37,44] of the conductance, a non self-consistent, step-function pair potential has been assumed. This neglects the very proximity effects which act on the singlet and triplet pair amplitudes, and thus the pair potential. In order to properly take these into account, one must use a self-consistent calculation of the pair potential. Even more important, only a self-consistent solution can guarantee that the conservation laws are satisfied[8], as we review in Sec. II below. The feasibility of the methods we use here was demonstrated in previous work[8] on simple $F/F/S$ heterostructures without N spacers or interfacial scattering, at $T = 0$. That work proved that the self-consistent BTK method embedded into a transfer matrix procedure can be used to calculate the tunneling conductance as well as the spin transport quantities. Our work presented here exploits these methods with a broader focus on realistic experimental parameters and sample compositions.

Because of the oscillatory nature of the superconducting singlet (and triplet) amplitudes in the F layers, we will see that, as expected, the transport results are highly dependent on the layer thicknesses, as they are on the exchange field.

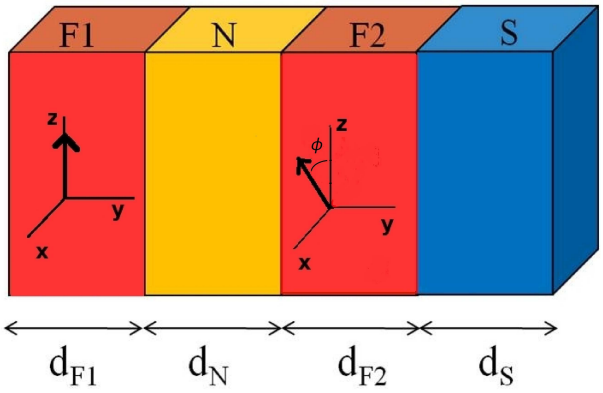

FIG. 1. (Color online) Sketch of the structures studied. The notation for thicknesses of the different layers is indicated, but the plot is not to scale. The y axis is normal to the layers. The magnetizations of the outer magnetic layer F_1 is along the z axis while in F_2 it is in the $x-z$ plane, forming an angle ϕ with the z axis, as indicated.

We report on the ϕ dependence of the tunneling conductance as the angular spin valve effect of the system. We do so for a variety of thicknesses for the ferromagnetic and normal layers. Furthermore, we investigate the dependence of G on the interfacial scattering strengths at all the interfaces. The dependencies that we find are, as a rule, nonmonotonic, and therefore straightforward extrapolations are not possible. Our goal is to provide a better understanding on the full range of experimentally relevant results where the interfacial quality cannot be perfectly controlled. From this, not only can one determine how these parameters affect the spin valve effect, but one can also provide the approximate set of parameters that can then maximize this effect: this has both experimental and technological importance. We investigate also, in a more restricted set of cases, the spin current and spin-transfer torque (STT).

After this Introduction, we briefly review our methods (both for equilibrium and transport calculations) in Sec II. The results are presented, chiefly in graphical form, in Sec. III, and discussed in the proper context. A summary Sec. IV closes the paper.

II. METHODS

A. The basic equations

The basic methods and procedures used are straightforward extensions of those discussed in Ref. 8 and they need not to be described again here. We merely sketch the main points, in order to establish notation and to make the paper understandable. The geometry of the system under consideration is represented qualitatively in Fig. 1. The layers are assumed to be infinite in the transverse direction. The y-axis is normal to the layers: this somewhat unconventional choice turns out to be computationally convenient because only the σ_y Pauli matrix is complex. The magnetizations of the outer and inner layers form an angle ϕ with each other.

The Hamiltonian appropriate to our system is,

$$\mathcal{H}_{eff} = \int d^3r \Bigg\{ \sum_{\alpha} \psi^{\dagger}_{\alpha}(\mathbf{r}) \mathcal{H}_0 \psi_{\alpha}(\mathbf{r}) + \frac{1}{2}\Bigg[\sum_{\alpha,\beta} \left(i\sigma_y\right)_{\alpha\beta} \Delta(\mathbf{r}) \psi^{\dagger}_{\alpha}(\mathbf{r}) \psi^{\dagger}_{\beta}(\mathbf{r}) + H.c. \Bigg] - \sum_{\alpha,\beta} \psi^{\dagger}_{\alpha}(\mathbf{r}) (\mathbf{h}\cdot\boldsymbol{\sigma})_{\alpha\beta} \psi_{\beta}(\mathbf{r}) \Bigg\}, \quad (1)$$

where $\Delta(\mathbf{r})$ is the pair potential and $\mathbf{h}$ is the usual Stoner field, which we take to be along the z axis (see Fig. 1) inside the outer magnet F_1, while forming an angle ϕ with the z axis in the $x-z$ plane inside the inner magnet F_2. We assume $h_1 = h_2 \equiv h$ since in most experiments the same material is employed. The field vanishes in the superconductor S and in the normal spacer N. $\mathcal{H}_0$ is the single particle Hamiltonian, which we will take to include the interfacial scattering as explained below. Performing a generalized Bogoliubov transformation in the usual way, with the phase conventions of Ref. 8, and taking advantage of the quasi one dimensional geometry one can recast the eigenvalue equation corresponding to the Hamiltonian given by Eq. 1 as:

$$\begin{pmatrix} H_0 - h_z & -h_x & 0 & \Delta \\ -h_x & H_0 + h_z & \Delta & 0 \\ 0 & \Delta & -(H_0 - h_z) & -h_x \\ \Delta & 0 & -h_x & -(H_0 + h_z) \end{pmatrix} \begin{pmatrix} u_{n\uparrow} \\ u_{n\downarrow} \\ v_{n\uparrow} \\ v_{n\downarrow} \end{pmatrix} = \epsilon_n \begin{pmatrix} u_{n\uparrow} \\ u_{n\downarrow} \\ v_{n\uparrow} \\ v_{n\downarrow} \end{pmatrix}, \quad (2)$$

with the $u_{n\sigma}$ and $v_{n\sigma}$ being the usual position and spin dependent quasiparticle and quasihole amplitudes involved in the transformation. We use units such that $\hbar = k_B = 1$. The quasi one dimensional Hamiltonian is $H_0 = -(1/2m)(d^2/dy^2) + \epsilon_{\perp} - E_F(y) + U(y)$ where $\epsilon_{\perp}$ is the transverse energy, (so that the above Eq. (2) is a set of decoupled equations, one for each $\epsilon_{\perp}$), $E_F(y)$ is the layer dependent width of the band: $E_F(y) = E_{FS} \equiv k^2_{FS}/2m$ in the S layer and $E_F(y) = E_{FM}$ in the F layers. We define a mismatch parameter[45] Λ as $E_{FM} \equiv \Lambda E_{FS}$. $U(y)$ is the interfacial scattering. We take this scattering, due to unavoidable surface roughness at the interfaces, to be spin-independent and of the form $U(y) = H_1\delta(y-d_{f1}) + H_2\delta(y-d_{f1}-d_N) + H_3\delta(y-d_{f1}-d_N-d_{f2})$. The dimensionless parameters $H_{Bi} \equiv H_i/v_F$, where v_F is the Fermi speed in S, conveniently characterize the strength of the delta functions.

All calculations must be performed self-consistently, otherwise a large part of the proximity effect is eliminated from the problem. As previously shown[8,46–48], and as reiterated in Section II C, it is paramount to perform the transport calculations self-consistently: not doing so jeopardizes the law of conservation of change[49]. The self consistency condition is:

$$\Delta(y) = \frac{g(y)}{2} \sum_n{}' \left[u_{n\uparrow}(y) v^*_{n\downarrow}(y) + u_{n\downarrow}(y) v^*_{n\uparrow}(y) \right] \tanh\left(\frac{\epsilon_n}{2T}\right), \quad (3)$$

where the sum is over all the eigenvalues and the prime in the sum denotes, as usual, that the sum is limited to states with eigenenergies within a cutoff ω_D from the Fermi level. The superconducting coupling constant $g(y)$, in the singlet channel, is nonvanishing in S only. Self consistency is achieved by starting with a suitable choice of $\Delta(y)$ and iterating Eqs. (2) and (3) until the input and output values of $\Delta(y)$ coincide. The thermodynamic quantities can then be derived from the wave functions. The transition temperature itself can be most conveniently obtained by linearization of Eq. (3) and an efficient eigenvalue technique[10,16] as in previous[32] work.

B. Transport: the BTK method and self-consistency

After the self consistent $\Delta(y)$ function has been obtained as reviewed above, one can proceed with the calculation of the transport properties. There are no fundamental difficulties in extending the self consistent[8] BTK method[38] to the case where an extra N layer and interfacial scattering exists. This is because the only nontrivial part of the transfer matrix procedure is that which deals with the self consistent pair potential inside S and this is extensively discussed in previous[8] work. For the rest, one has of course additional matching equations at the two added interfaces. The matching equations are of the same basic form as those found previously[8] except for the interfacial scattering, which requires, as in elementary situations, a modification of the derivative continuity condition. Again, it is not necessary to discuss here these relatively elementary questions, although care is required to include them correctly in the computations. We confine ourselves to the minimum necessary to make the notation clear.

For an incident particle with spin up the wavefunction in F_1 is:

$$\Psi_{F1,\uparrow} \equiv \begin{pmatrix} e^{ik^+_{\uparrow 1}y} + b_{\uparrow} e^{-ik^+_{\uparrow 1}y} \\ b_{\downarrow} e^{-ik^+_{\downarrow 1}y} \\ a_{\uparrow} e^{ik^-_{\uparrow 1}y} \\ a_{\downarrow} e^{ik^-_{\downarrow 1}y} \end{pmatrix}. \quad (4)$$

where we have include the appropriate amplitudes for the ordinary and Andreev reflection processes, which we must calculate. If the incident particle has spin down, the corresponding wavefunction in F_1 is

$$\Psi_{F1,\downarrow} \equiv \begin{pmatrix} b_{\uparrow} e^{-ik^+_{\uparrow 1}y} \\ e^{ik^+_{\downarrow 1}y} + b_{\downarrow} e^{-ik^+_{\downarrow 1}y} \\ a_{\uparrow} e^{ik^-_{\uparrow 1}y} \\ a_{\downarrow} e^{ik^-_{\downarrow 1}y} \end{pmatrix}. \quad (5)$$

with appropriate amplitude coefficients, numerically different from those for the spin up incident particle. One has, in the above equations:

$$k^{\pm}_{\sigma 1} = \left[\Lambda(1 - \eta_{\sigma} h_1) \pm \epsilon - k^2_{\perp} \right]^{1/2}, \quad (6)$$

where $\eta_\sigma \equiv 1(-1)$ for up (down) spins, and $k_\perp$ is the length of the wavevector corresponding to energy $\epsilon_\perp$. All wavevectors are understood to be in units of k_{FS} and all energies in terms of E_{FS}.

All of the amplitudes are then determined from the transfer matrix procedure discussed in Ref. 8, where the self-consistent pair potential determines the wavevectors in the S layer. The transfer matrix matches the continuity conditions for each layer. The outcome of the calculations includes the reflection amplitudes a_σ and b_σ of the incoming wavefunctions for the different (ordinary and Andreev, spin up and spin down) reflection processes. From these the conductance is extracted as explained below.

C. Conservation laws and conductance

In transport calculations great care has to be taken not to violate[49] the conservation laws. Consider the equation for charge density $\rho(\mathbf{r}, t)$ which arises from the Heisenberg equation:

$$\frac{\partial}{\partial t}\langle\rho(\mathbf{r})\rangle = i\left\langle\left[\mathcal{H}_{eff}, \rho(\mathbf{r})\right]\right\rangle. \tag{7}$$

We are considering here steady state situations, so the time derivative vanishes and we simply should have a zero a divergence condition for the current. In our quasi two dimensional geometry, the only non-vanishing component of the current is j_y, and it depends only on y. Hence we need to ensure that $\partial j_y/\partial y = 0$. Upon computing the commutator in the right side of Eq. (7) under these conditions we find, however:

$$\frac{\partial j_y(y)}{\partial y} = 2e\mathrm{Im}\left\{\Delta(y)\sum_n\left[u^*_{n\uparrow}v_{n\downarrow} + u^*_{n\downarrow}v_{n\uparrow}\right]\tanh\left(\frac{\epsilon_n}{2T}\right)\right\} \tag{8}$$

In transport calculations the wavefunctions cannot be taken to be real, as is possible for the evaluation of static quantities in a current-free situation. Hence it is not necessarily true that the right side of Eq. (8) will vanish. However, it is easy to see[9,47] that it will be identically zero when the self consistency condition Eq. (3) is satisfied. Therefore, the importance of performing the calculations self consistently, despite the computational simplifications inherent to non-self-consistent methods, cannot be overemphasized.

D. Extraction of the conductance

From the results of the previous subsection, one can extract the conductance. The current is related to the applied bias[38] V via the expression:

$$I(V) = \int G_0(\epsilon)\left[f(\epsilon - eV) - f(\epsilon)\right]d\epsilon, \tag{9}$$

where f is the Fermi function. The bias dependent tunneling conductance is $G(V) = \partial I/\partial V$. The function G_0 in Eq. (9) is the conductance in the low-T limit or, more generally, the conductance obtained by replacing the derivative of the Fermi function by a δ function. It is related to the scattering amplitudes by:

$$G_0(\epsilon,\theta_i) = \sum_\sigma P_\sigma G_\sigma(\epsilon,\theta_i) \tag{10}$$
$$= \sum_\sigma P_\sigma\left(1 + \frac{k^-_{\uparrow 1}}{k^+_{\sigma 1}}|a_\uparrow|^2 + \frac{k^-_{\downarrow 1}}{k^+_{\sigma 1}}|a_\downarrow|^2 - \frac{k^+_{\uparrow 1}}{k^+_{\sigma 1}}|b_\uparrow|^2 - \frac{k^+_{\downarrow 1}}{k^+_{\sigma 1}}|b_\downarrow|^2\right),$$

in the customary natural units of conductance (e^2/h). In Eq. (10) the different k symbols are as defined in Eq. (6). The angle θ_i is the angle of incidence: for spin up it is given by $\tan\theta_i = (k_\perp/k^+_{\uparrow 1})$, and similarly for spin down. Thus one has $\theta_i = 0$ for the forward conductance. The factors $P_\sigma \equiv (1 - h_1\eta_\sigma)/2$ are included to take into account the different density of incoming spin up and spin down states. The energy dependence of $G(\epsilon)$ arises from the applied bias voltage V. It is customary and convenient to measure this bias in terms of the dimensionless quantity $E \equiv eV/\Delta_0$ where Δ_0 is the value of the order parameter in bulk S material. We will refer to the dimensionless bias dependent conductance simply as $G(V)$ or $G(E)$ usually omitting the angular argument.

One can not always assume that the experiments are performed in the low T limit. At finite temperature there are two sources of T corrections. The first and more obvious is that arising from the T dependence of $\Delta(y)$, that is, the T dependence of the effective BCS Hamiltonian. This is of course straightforward to include: one just calculates the self consistent Δ at finite T (see Eq. (3) and uses it as input in the transfer matrix calculations. But there is also a temperature dependence arising from the Fermi function in Eq. (9). If the temperature is not too close to T_{c0}, the transition temperature of the bare S material, which sets the overall scale, one can use a Sommerfeld type expansion. Because the energy scale over which $G(V)$ varies is of order Δ_0, the relevant expansion parameter is T/T_{c0}, not T/T_F, and hence not necessarily negligibly small in all experimental situations. One finds using elementary[50] methods:

$$G(V,T) = G_0(V) + a_1\left(\frac{T}{\Delta_0}\right)^2\left(\frac{\partial^2 G(V)}{\partial\epsilon^2}\right)\Big|_{\epsilon=V} + O\left(\frac{T}{\Delta_0}\right)^4 \tag{11}$$

where a_1 can be expressed[50] in terms of a Bernoulli number. Alternatively, one can use the general form:

$$G(V,T) = \frac{1}{4T}\int dV' \frac{1}{\cosh^2[(1/2T)(V - V')]}G_0(V'). \tag{12}$$

In Eqs. (11) and (12) $G_0(V)$ means the result of Eq. (10) evaluated with the self consistent pair potential at temperature T. The second form turns out to be more useful as most relevant temperatures turn out to be too high for the Sommerfeld expansion.

E. Spin transport

We will consider also spin transport across the junction. In our quasi one-dimensional geometry the tensorial spin current

becomes a vector in spin space, while spatially it depends only on y. Denoting this vector as $\vec{S}(y)$ it can be written[8] in terms of the wavefunctions, as:

$$S_i \equiv \frac{i\mu_B}{2m}\sum_\sigma \left\langle \psi^\dagger_\sigma \sigma_i \frac{\partial \psi_\sigma}{\partial y} - \frac{\partial \psi^\dagger_\sigma}{\partial y}\sigma_i \psi_\sigma \right\rangle . \tag{13}$$

It is not difficult to write the components S_i in terms of the u_n and v_n wavefunctions. In the $T = 0$ limit, the result is:

$$S_x = \frac{-\mu_B}{m}\mathrm{Im}\left[\sum_n \left(-v_{n\uparrow}\frac{\partial v^*_{n\downarrow}}{\partial y} - v_{n\downarrow}\frac{\partial v^*_{n\uparrow}}{\partial y}\right)\right. \tag{14a}$$
$$\left. + \sum_{\epsilon_{\mathbf{k}}<eV}\left(u^*_{\mathbf{k}\uparrow}\frac{\partial u_{\mathbf{k}\downarrow}}{\partial y} + v_{\mathbf{k}\uparrow}\frac{\partial v^*_{\mathbf{k}\downarrow}}{\partial y} + u^*_{\mathbf{k}\downarrow}\frac{\partial u_{\mathbf{k}\uparrow}}{\partial y} + v_{\mathbf{k}\downarrow}\frac{\partial v^*_{\mathbf{k}\uparrow}}{\partial y}\right)\right]$$
$$S_y = \frac{\mu_B}{m}\mathrm{Re}\left[\sum_n \left(-v_{n\uparrow}\frac{\partial v^*_{n\downarrow}}{\partial y} + v_{n\downarrow}\frac{\partial v^*_{n\uparrow}}{\partial y}\right)\right. \tag{14b}$$
$$\left. + \sum_{\epsilon_{\mathbf{k}}<eV}\left(u^*_{\mathbf{k}\uparrow}\frac{\partial u_{\mathbf{k}\downarrow}}{\partial y} + v_{\mathbf{k}\uparrow}\frac{\partial v^*_{\mathbf{k}\downarrow}}{\partial y} - u^*_{\mathbf{k}\downarrow}\frac{\partial u_{\mathbf{k}\uparrow}}{\partial y} - v_{\mathbf{k}\downarrow}\frac{\partial v^*_{\mathbf{k}\uparrow}}{\partial y}\right)\right]$$
$$S_z = \frac{-\mu_B}{m}\mathrm{Im}\left[\sum_n \left(v_{n\uparrow}\frac{\partial v^*_{n\uparrow}}{\partial y} - v_{n\downarrow}\frac{\partial v^*_{n\downarrow}}{\partial y}\right)\right. \tag{14c}$$
$$\left. + \sum_{\epsilon_{\mathbf{k}}<eV}\left(u^*_{\mathbf{k}\uparrow}\frac{\partial u_{\mathbf{k}\uparrow}}{\partial y} - v_{\mathbf{k}\uparrow}\frac{\partial v^*_{\mathbf{k}\uparrow}}{\partial y} - u^*_{\mathbf{k}\downarrow}\frac{\partial u_{\mathbf{k}\downarrow}}{\partial y} + v_{\mathbf{k}\downarrow}\frac{\partial v^*_{\mathbf{k}\downarrow}}{\partial y}\right)\right],$$

where the first terms in the right side are the spin current components in the absence of bias. A static spin transfer current may exist near the boundary of two magnets with misaligned fields. The above results are valid at low T, we will not consider temperature corrections for this quantity. In the steady state the conservation laws require:

$$\frac{\partial}{\partial y}S_i = \tau_i, \quad i = x, y, z \tag{15}$$

where $\boldsymbol{\tau}$ is the torque $\boldsymbol{\tau} \equiv 2\mathbf{m}\times\mathbf{h}$ with $\mathbf{m}$ being the local magnetization $\mathbf{m} = -\mu_B\sum_\sigma\langle\psi^\dagger_\sigma\boldsymbol{\sigma}\psi_\sigma\rangle$. The expression for $\mathbf{m}$ in terms of the wavefunctions is given in Ref. 8.

III. RESULTS

In this section we present our results. As discussed in the Introduction, our emphasis is in exploring a range of values of experimental interest for the relevant parameters. This, in addition to helping us meet our goal of helping experimentalists understand their data, will keep the discussion within reasonable bounds: otherwise, with a more than ten-dimensional parameter space to be investigated, this work would completely lose its focus. We do have an extensive and growing database of results for many other cases. As mentioned above, we use dimensionless parameters in our plots: all lengths are given in units of k_{FS} and all energies in units of E_{FS} except, as already stated, for the bias. Dimensionless lengths will be

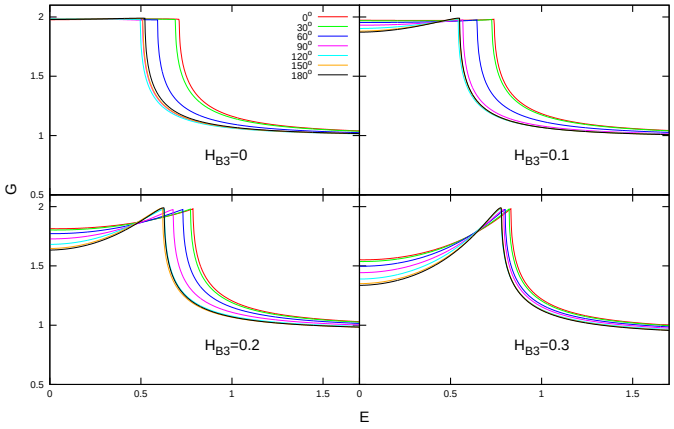

FIG. 2. Effect on the conductance of the barrier between the superconductor and the inner ferromagnet H_{B3}. The four panels show results for G in natural units, as a function of bias voltage $E \equiv eV/\Delta_0$ at seven values of the misalignment angle ϕ as indicated in the legend. The panels correspond to different values of H_{B3} ranging from 0.0 to 0.3 with $H_{B1} = H_{B2} \equiv H_B = 0$. The thicknesses are $D_{F1} = 20$, $D_N = 40$, $D_{F2} = 12$ and $D_S = 180$. The internal field parameter is $h = 0.145$

denoted by capital letters with the appropriate subscript. The units for the dimensionless barrier height parameters H_{Bi} have been explained before. Values close to unity would represent a strong tunneling limit: these would be experimentally very undesirable as the proximity effects would be very small. Zero values represent an ideal interface, which is unlikely to be attainable experimentally. Since the first and second interfaces are both between F and N materials, one can fairly safely assume that these two barrier strengths are similar, and we will usually take them to be identical, $H_{B1} = H_{B2} \equiv H_B$. In our dimensionless units a field parameter value of $h = 1$ would correspond to a half metal. The results for G presented are for $h = 0.145$ a value previously found adequate[32] in fitting Co static properties in similar devices. As in Ref. 32 we set $\Lambda = 1$, which subsumes some of the wavevector mismatch effects with the phenomenologial H_{Bi} parameters. We will also assume a value of $\Xi_0 = 115$ for the dimensionless correlation length in S, a value used in the same context[32] for Nb. We will vary the thicknesses of all layers, keeping D_{F2} relatively small, which is necessary to obtain good proximity effect, and allowing D_N and D_{F1} to be somewhat larger. As to D_S, the thickness of the superconducting layer, it must of course be kept above Ξ_0: otherwise the sample tends to become non-superconducting, for rather obvious reasons. We will focus here on forward conductance results, which can be obtained from point probes and involve trends much easier to understand.

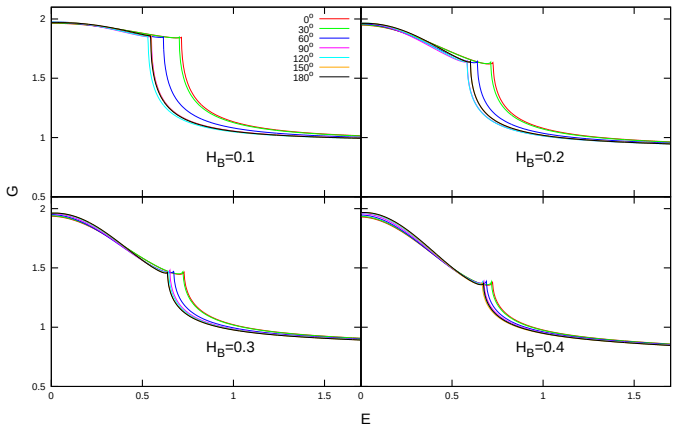

FIG. 3. Effect on the conductance of the barriers between the normal spacer and the ferromagnets $H_{B1} = H_{B2} = H_B$. The four panels show results for the same arrangement as in Fig. 2 and the same geometrical and field parameters except in this case H_{B3} is held constant and the value of the barrier parameter at the other two interfaces is varied between 0.1 and 0.4.

A. Barrier effects

The effects of interfacial scattering are very strong and important. Recall that even in standard normal-superconductor interfaces the zerto bias conductance (ZBC) can vary between a value of two for a perfect interface, and an exponentially small value for the tunneling limit. One should recall here that even in the case where a certain barrier parameter vanishes, there is still scattering at the correspondent interface: this is because it is impossible for the two Fermi wavectors in the ferromagnets to match the Fermi wavevector of either the N or the S materials. This has to be kept in mind in the discussion below.

In Fig. 2 we show the effect of increasing H_{B3} assuming that the other interfaces have zero interfacial potential, although scattering due to wavevector mismatches is present. Four values of H_{B3} are studied, one in each panel, and curves for seven values of the misalignment angle ϕ are plotted. The geometrical parameters are $D_{F1} = 20$, $D_N = 40$, $D_{F2} = 12$ and $D_S = 180$. The overall trend on increasing H_{B3} is a marked decrease of the low bias conductance and a much smaller decrease of the high bias limiting value. The critical bias (CB) is the value of the bias at which G sharply changes behavior and begins trending towards its normal state limit. In general, the critical bias is smaller than unity, and smaller values are associated with stronger proximity effects since the CB is associated with the saturated value of $\Delta(Y)$ well inside S. We see that the CB tends to increase with H_{B3}, while the value of G at critical bias (the critical bias conductance, CBC) remains nearly the same. On the other hand, the CB is in all cases a strong function of ϕ, decreasing as ϕ increases, up to about $\phi = 100^\circ$ and then flattening, for this geometry. The dependence is less marked at higher barrier values. The ZBC however, is monotonically decreasing in ϕ. This dependence on ϕ is different from that of the CB or CBC, and it leads to a crossover in the conductance values. Remarkably, this crossover tends to occur with a "nodal" behavior at a single bias value in the subgap region: this can best be seen in the third and fourth panels. Monotonic behavior in the ZBC also occurs for other values of D_{F2} that we have studied, but the direction (increasing or decreasing in ϕ) is reversed in an oscillatory way: for example the ZBC increases with ϕ at values of D_{F2} of 7 and 10 and again at 16,17. This is one more example of the multiple oscillatory behavior found in this problem and an illustration of how much care one has to take before extrapolating results.

Next we consider, in Fig. 3, the effect of increasing $H_{B1} = H_{B2} \equiv H_B$ while keeping $H_{B3} = 0$ at the F_2/S interface. Again, four barrier values are considered, in an arrangement very similar to that in the previous figure. The effects of interfacial scattering are now more pronounced. This is not necessarily due to the presence of two barriers: as in well known situations in elementary one-dimensional quantum mechanics, we find that having more barriers does not necessarily lead to less transparency. This analogy is imperfect: our system is not one-dimensional, there are multiple scattering mechanisms (interfacial imperfections, wavevector mismatch, Andreev reflection, etc). Still, we find that having two barriers does not always reduce transmission. A clear example of this can be seen in the ZBC value which, for the chosen values of $D_{F2} = 12$ and D_N, is nearly independent of H_B. This is because of resonance-like behavior in this geometry. Furthermore, changing the values of $D_{F2} = 12$ and D_N leads to ZBC behavior more similar to that in Fig. 2, which we discuss in the next subsection in connection with Fig. 6. The behavior of the CB with angle is nonmonotonic, in a way similar to that found in Fig. 2. The minimum is now somewhat less shallow, particularly at higher H_B. At low bias, G decreases as the bias is increased, although an upturn does occur as the CB is approached albeit at a lower value of the CBC for increasing H_B. This is in contrast to Fig. 2 where the CBC was unaffected by H_{B3}.

B. Geometrical Effects

We have mentioned in the previous discussion that the thickness of the different layers may have a strong and often nonmonotonic effect on G. The thickness of the inner magnetic layer, D_{F2} turns out to be the more important of these geometrical variables. In the six panels in Fig. 4 we consider increasing values of D_{F2} while keeping the other geometrical and material parameters fixed to their values in the previous figures. The three interfacial barrier parameters are set to intermediate values (see the caption).

Consider in detail the first panel, where $D_{F2} = 7$. One notices immediately the reduction in ZBC, as opposed to the results for $D_{F2} = 12$ in the third panel or to those in the previous figures. The behavior of this reduction occurs, as has been mentioned above, in an oscillatory manner with D_{F2}: it

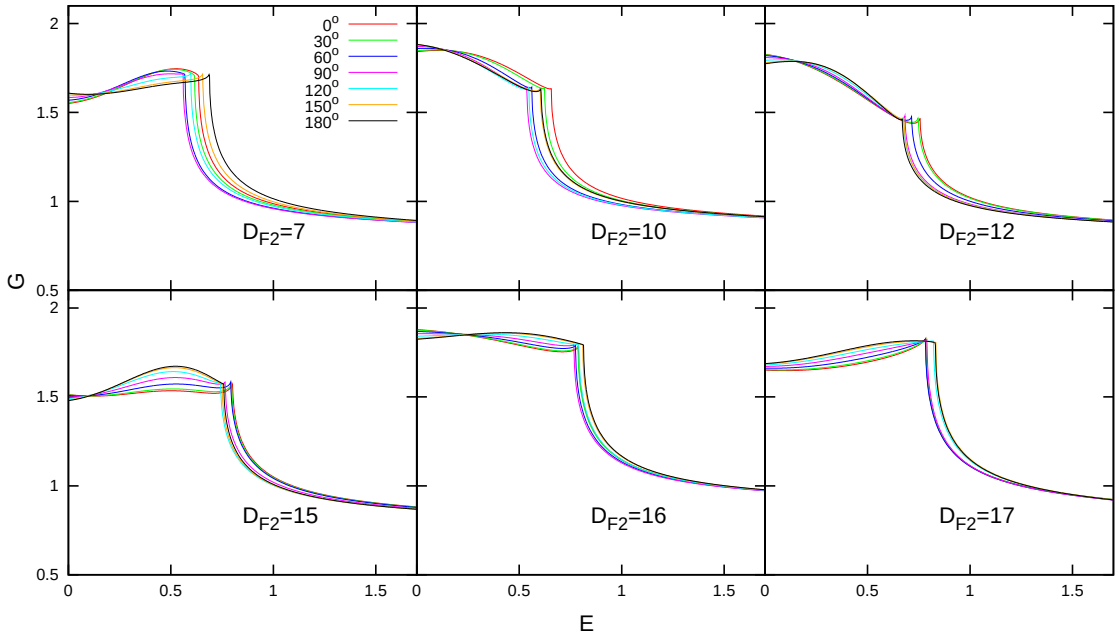

FIG. 4. Effect on the conductance by varying the thickness D_{F2} of the inner ferromagnetic layer. The values of the other thicknesses, field, and correlation length are as in the previous two figures, and the barrier values are set to 0.3, 0.3, and 0.1 respectively, which are representative of possible experimental values. The six panels show G vs bias voltage for several angles, at six values of $D_{F2} = 7, 10, 12, 15, 16$, and 17. The spin valve effect varies significantly in both the CB and the ZBC.

can be seen again at $D_{F2} = 15$ (fourth panel). In this panel, as in the second and the fifth, the minimum value of the CB with angle is at $\phi = 90°$, and this minimum is very well marked – this is an optimum situation for valve effects. The ZBC value depends somewhat on ϕ but not in the same way as the CB: hence, the crossing conductance curves near a bias of 0.2. The second panel exhibits similar behavior, but the ZBC is markedly higher. On further increasing D_{F2} to 12 (third panel) the CB becomes monotonic in ϕ while the low bias conductance does not change: indeed the node where the lines cross barely moves. The case $D_{F2} = 15$ (fourth panel) is yet different: the CB is larger and there is a marked "bump" in the low bias conductance, the height of which increases with ϕ. Resonance in the ZBC is observed again in the fifth panel, and the angular dependence of the CB returns to having a marked minimum at $\phi = 90°$ although with a weaker dependence. Furthermore, the node noticeably moves to a higher bias value. Finally, at $D_{F2} = 17$ (last panel) the ZBC drops again, the angular dependence of the CB is reversed, and the node disappears. Thus we see that the thickness of the inner magnetic layer is a very important variable in determining the conductance properties.

On the other hand, the effect of varying D_{F1}, the thickness of the outer ferromagnetic layer, is much weaker than that of varying D_{F2}. This is illustrated in the first two panels of Fig. 5. There we display, in each panel, results for G at fixed $\phi = 0$. In the first panel we do this for several values of D_{F1} ranging from 12 to 30 and, in the second panel, for D_{F2} values from 7 to 17 at fixed D_{F1}. In both panels $D_N = 40$. Barrier heights and other parameters are as in Fig. 4. The difference is obvious: while in the first panel the results barely change (although the change is nonmonotonic), in the second one every relevant quantity (CB, ZBC, high bias and low bias behaviors etc) changes, in obvious and very strongly nonmonotonic ways. Thus, in the fabrication process, the precise thickness of D_{F1} is less critical than that of D_{F2}. As to the normal spacer thickness, in the last two panels of Fig. 5 we consider the dependence of G on D_N. We again plot G at fixed $\phi = 0$ for several values of D_N at two values of D_{F2} (see caption). One can see that while quantities such as the CB do not depend very much on D_N, the low and high bias behaviors vary quite appreciably overall, the former rather dramatically. Hence we conclude that D_{F2} is the crucial geometrical parameter in the problem, followed in importance by D_N and with D_{F1} being much less relevant.

Careful examination of the above results yields insights on the combined effects of interfacial scattering and on geometry, particularly on D_{F2}: how geometry and interfacial strength are related follows ultimately from the oscillatory nature of the Cooper pairs and from quantum mechanical interference. We now display, in Fig. 6, these combined effects in a more direct way. As in Fig. 5 we study results for fixed $\phi = 0$. We consider four values of D_{F2}, one in each panel, ranging from 7 to 17, and plot results for several values of H_B at $H_{B3} = 0$. In the first panel we see a large and monotonic dependence on H_B of the entire conductance dependence. In the next case shown,

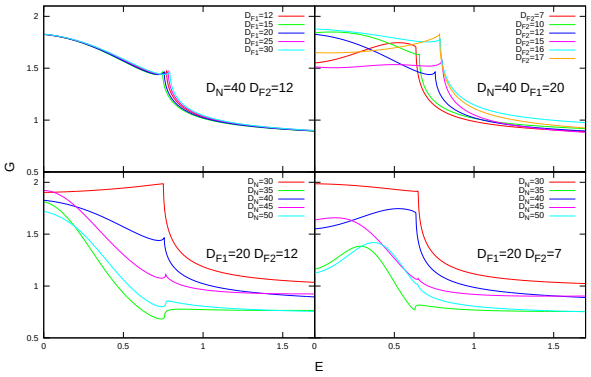

FIG. 5. Effects of varying D_{F1} or D_N, compared with dependence on D_{F2}. All panels are for $\phi = 0$, barrier values of 0.3, 0.3, and 0.1 and the field parameter, correlation length, and D_S are as in Figure 2. The first two panels contrast the effect on the conductance of varying the thickness D_{F1} of the outer ferromagnetic layer with D_{F2} of the inner ferromagnetic layer. In the first panel, D_{F1} is varied, as indicated in the legend, at $D_{F2} = 12$, while in the second one D_{F2} is varied at $D_{F1} = 20$. The last two panels show the effect of varying D_N at $D_{F1} = 12$ and $D_{F2} = 7$ respectively. The dependence of the results on D_{F1} is much weaker than that on D_{F2} or D_N. Both D_{F2} and D_N have a large impact on the ZBC, meanwhile D_{F2} has a much larger effect on the CB.

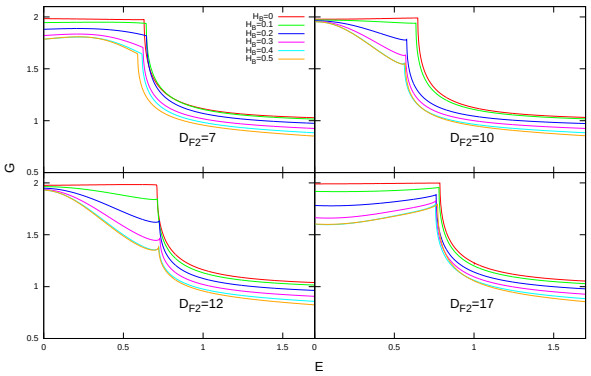

FIG. 6. Combined effect of D_{F2} and barriers. The behavior at fixed $\phi = 0$ and $H_{B3} = 0$ is studied. Each of the four panels corresponds to a fixed value of D_{F2}: 7, 10, 12, and 17 and the curves correspond to values of $H_{B1} = H_{B2} \equiv H_B$ as indicated in the legend. A nonmonotonic feature in the ZBC is observed as a function of D_{F2}, owing to the oscillatory behavior of the Cooper pairs.

$D_{F2} = 12$, the ZBC depends only very weakly on H_B. In the next panel, the spread in the ZBC with ϕ increases somewhat, as compared to the previous panel, and it does so even more in the last panel. This resonance-like behavior is not the same as in the one-dimensional two barrier problems in basic quantum mechanics, where a resonance feature is observed in the

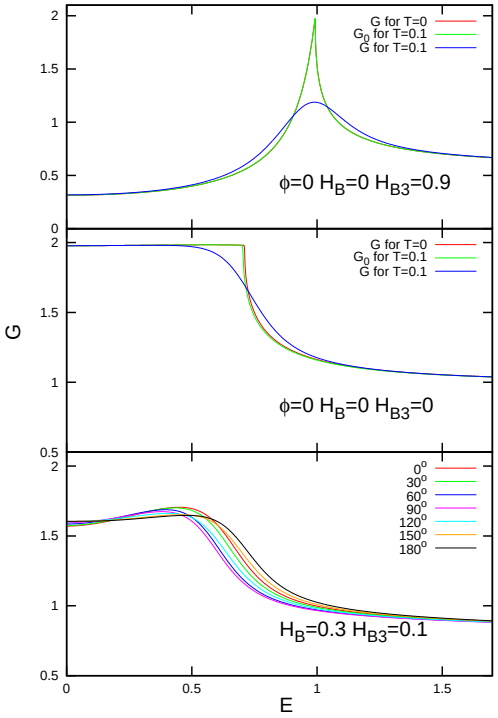

FIG. 7. Temperature dependence of the conductance. In the first two panels we consider G at fixed ϕ. The thicknesses and fields are as in Fig. 2. Temperatures $T = 0.1$, in units of T_{c0}, are compared to $T = 0$ results. The result of including only G_0, the correction to G arising from the T dependence of $\Delta(y)$ is also shown. The first panel is for a very high barrier ($H_{B3} = 0.9$) between S and F_2 and $H_{B1} = H_{B2} = 0$, while in the second all $H_{Bi} = 0$. The G_0 result at $T = 0.1$ is nearly identical to the G at $T = 0$. The last panel illustrates (for the same values as the first panel in Fig. 4), a case where the CB varies very nonmonotonically with angle, and shows how little this behavior is affected by T.

transmission coefficients as a function of the distance between the barriers. This analogy might apply better to D_N, but not to the inner ferromagnetic thickness D_{F2}. Instead, this resonance is due to the oscillatory behavior of the Cooper pairs. We see then that certain values of D_{F2} make the system, or at least its ZBC, partly "immune" to the effects of fairly high surface barriers. Although this holds only to a limited extent, it may be worthwhile to attempt to exploit this effect to palliate the existence of unfavorable interfaces with unavoidably large scattering.

C. Temperature dependence

Experiments in these systems are not performed at zero temperature, nor, in practice, at ultralow T. Therefore the influence of T must be examined. There are two transition temperatures to consider: the transition temperature T_{c0} of pure bulk S material, and the transition temperature T_c of the device, which is typically considerably lower. In our discussion we will use a dimensionless temperature T in units of T_{c0}

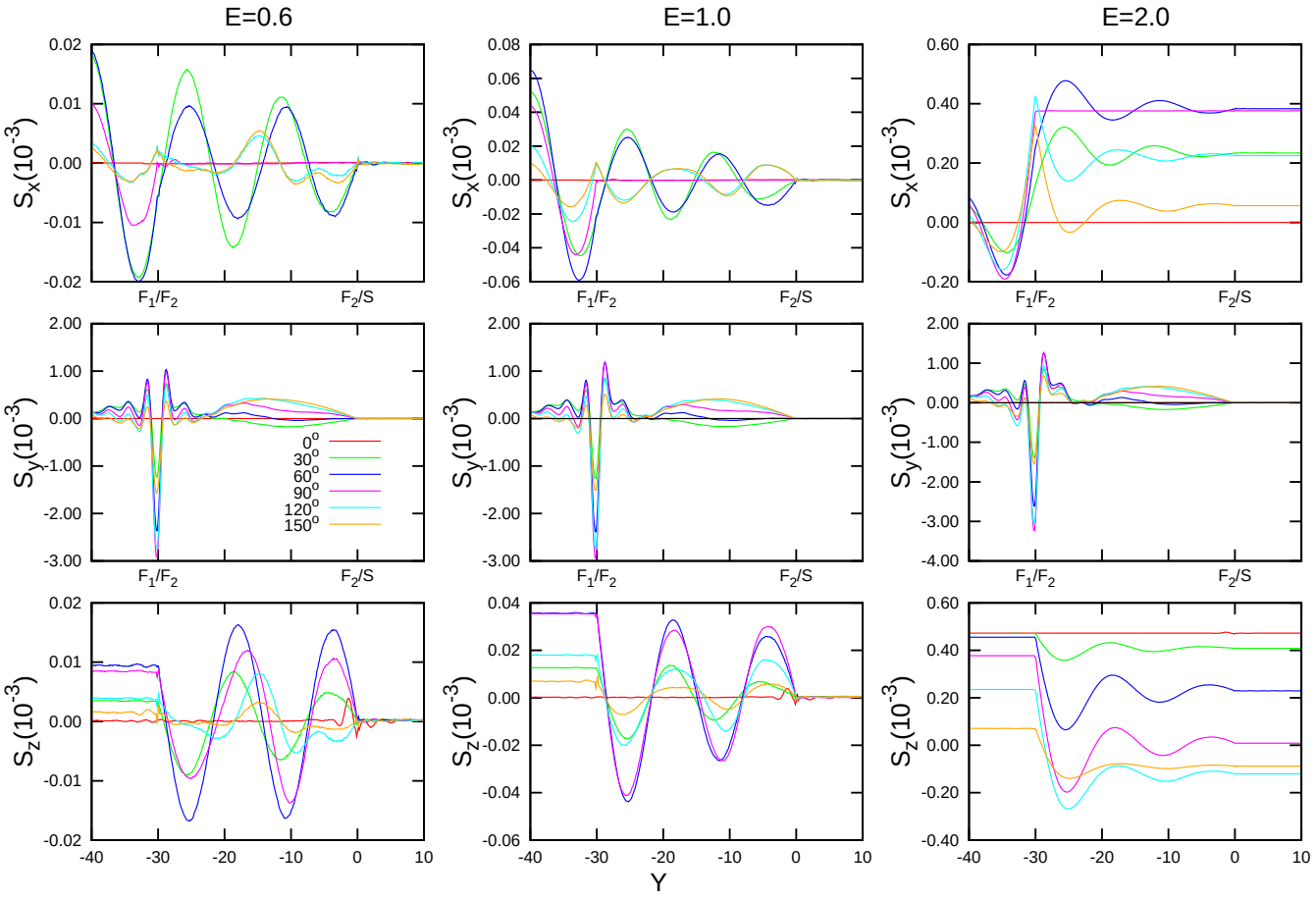

FIG. 8. The three components of the spin current are shown as a function of Y for several values of ϕ, as indicated, and three values of the bias voltage. We have $h = 0.1$, $D_{F1} = D_S = 250 = 5\Xi_0$, $D_{F2} = 30$, $D_N = 0$. Only the central region of Y is plotted: $Y = 0$ is at the F_2/S interface. All components of the spin current are zero for $\phi = 180°$.

since T_c varies as the geometry is changed.

As explained in Sec. II D one has to consider two sources of T dependence. The first is that arising from the self-consistent pair potential, $\Delta(y)$, that is, the T dependence in the effective Hamiltonian. This leads to the function G_0 defined below Eq. (9) and in Eq. (10) being T dependent. The second is that originating in the Fermi functions in Eq. (9). As discussed in connection with Eq. (11) the latter is not negligible since the scale of the variation of G with bias is Δ_0, not the Fermi energy. We have found that, in practice, Eq. (12), which is not dependent on any expansion, is much more useful than the Sommerfeld method in the relevant temperature range. This is because the conductance has large, and even discontinuous derivatives, which the Sommerfeld expansion does not handle well.

Representative results are shown in Fig. 7. In the first two panels we consider a fixed $\phi = 0$ and we show results for G both at $T = 0$ and at a reduced temperature $T = 0.1$. Since for the size ranges considered in this section we have found that T_c/T_{c0} values are in the 0.5 to 0.6 region, these correspond to T/T_c of about 0.2. The first panel shows results in a strong tunneling limit regime, with high barriers, and the second for zero barrier heights. Plots of G_0 , i.e. the results obtained by using the $\Delta(y)$ correction only are also included: these are obviously inadequate in both cases, and the full result is needed. We have found this to be invariably the case except at unrealistically low T. The overall effect of the temperature is, otherwise, that of rounding up and softening the sharp features of the low T results. A consequence of this is that at finite T one has to redefine more carefully the CB as the bias value at which G has a peak or a high derivative. The proper redefinition is the bias value at which G varies fastest.

In the third panel of Fig. 7, we replot G for the same case considered in the first panel of Fig. 4, which, as we have remarked before, shows good spin valve effects in its CB properties, but now at $T = 0.1$ instead of at zero temperature. The two results should be carefully compared. We see that while the curves are now much smoother the behavior of the different features with angle are robust. In particular the sharp minimum of the critical bias at $\phi = 90°$ remains unchanged. We have found this to be the the situation in all the cases we have checked. Hence, spin valve properties are only weakly dependent on T.

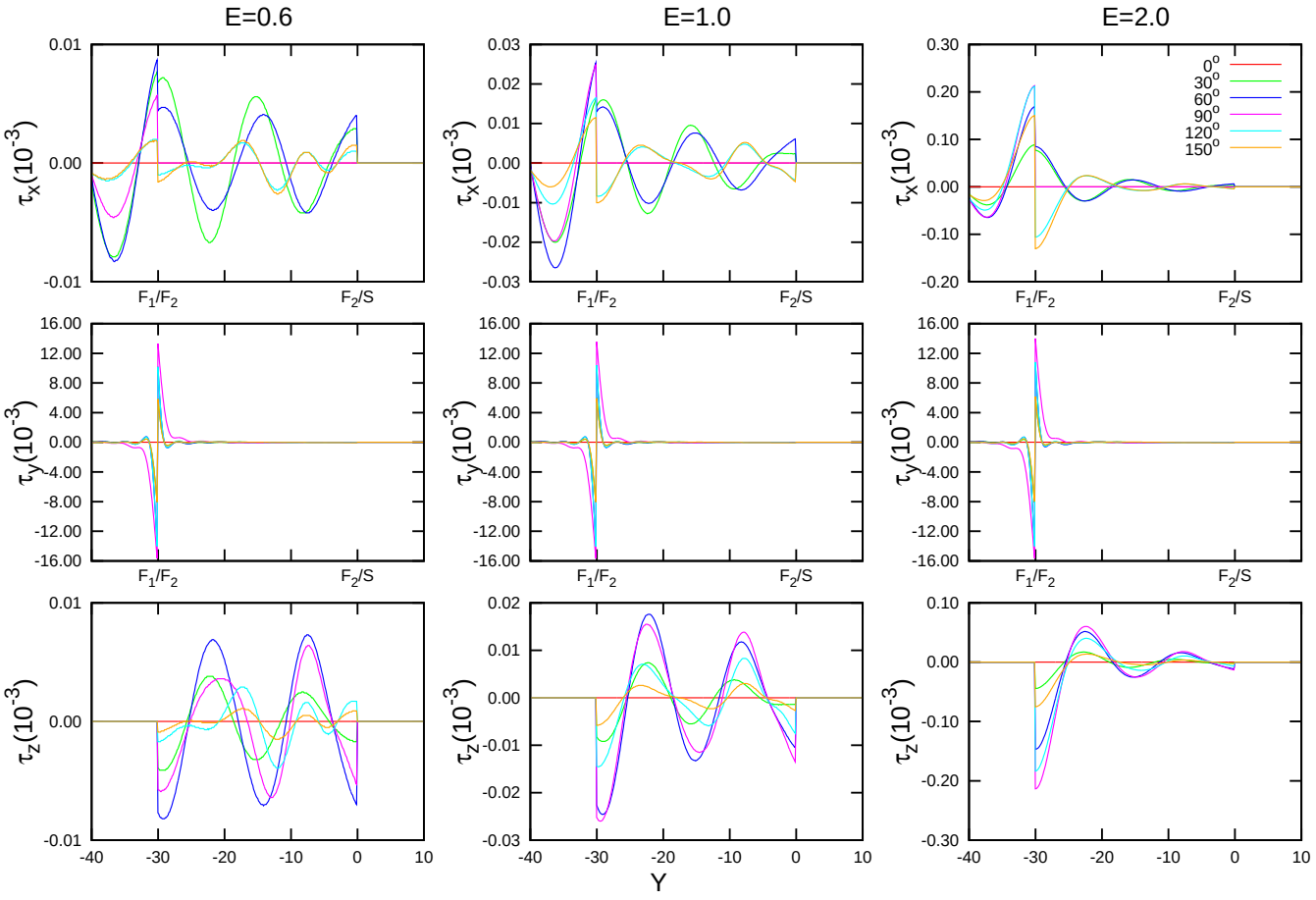

FIG. 9. The three components of the spin transfer torque plotted for the same situation as in the previous figure. The torque is identically zero for $\phi = 0$ and $\phi = 180^\circ$. The discontinuities at the interface reflect those of the internal fields.

D. Spin Currents

We present here some results for the spin current and the spin transfer torque. We restrict ourselves to the case where there is no spacer, and the barrier parameters are zero. However, we consider in this paper a range of bias voltages and all values of the angle ϕ. Very limited results for only $\phi = 90^\circ$ value were given in Ref. 8. We use units such that $\mu_B = 1$ and take $h = 0.1$. We consider a superconductor thickness of five times the coherence length ($D_S = 250 = 5\Xi_0$) so that the saturated value of $\Delta(y)$ is essentially the same as the bulk S value Δ_0. We assume a rather thick F_1 layer ($D_{F1} = 250$) while $D_{F_2} = 30$.

The main quantities we will focus on are the three components of the spin currents and of the spin transfer torques (STT) as a function of position. For the charge current, the conservation law entails that the current is independent of position. But for spin, the derivative of the current is the STT (see Eq. (15)) and the latter quantity is of great physical interest. As usual[8,19] we normalize $\mathbf{m}$ to $-\mu_B(N_\uparrow + N_\downarrow)$. The normalization for the spin current follows from these conventions. There are two alternative methods to calculate the spin currents: one is directly from the expressions in Eqs. (14). The other method is to calculate the torque first, from the expression below Eq. (15) and then integrate over the y variable. The two methods agree when the calculations are done self consistently, as was conclusively shown in Ref. 8. The second method is computationally much easier, but it yields results only up to a constant of integration. We have therefore used the direct method: it requires obtaining wavefunction results over a very fine mesh, so that the derivatives in Eq. (14) can be calculated to sufficient accuracy.

In the following discussion it is well to recall the meaning of the indices and coordinates. The spin current is in general a tensor, each element having two indices, one corresponding to the spatial components and the other to spin. In a quasi-dimensional geometry, the only spatial component is in the y direction, normal to the layers in our convention (see Fig. 1). The spin current is then simply a vector in spin space: the indices in S_i denote spin components, with all transport being in the spatial y direction. Recalling Eq. (15) and the definition of the torque $\tau = 2\mathbf{m}\times\mathbf{h}$ we see that τ_y tends to twist the magnetization in the plane of the layers, but of course it can only do so in regions near the interfaces, where $\mathbf{m}$ and $\mathbf{h}$ are not parallel due to magnetic proximity effects. We also see that

each component of the torque vanishes in the S layer where the internal field parameter h is zero.

We can now discuss the plots in Figs. 8 and 9. These two figures show results for the three components of the spin current and of the STT respectively, each under the same conditions (see captions). These quantities are shown for three values of the bias, E, ranging from below to well above Δ_0: for each component, there is a panel corresponding to each value of E. The curves correspond to different values of ϕ as indicated in the legend. At $\phi = 0$ and $\phi = 180^\circ$ the same conservation laws that preclude singlet to triplet pair conversion imply that the torques vanish. It is evident that there is no point in including the regions of the sample deep inside S or even well inside F_1, so the region plotted is that which includes both interfaces: the S/F_2 interface at the origin and that between ferromagnets at $Y = -30$, where Y is the dimensionless position.

The y-components results are easiest to understand: the component of the torque has very sharp peaks, with opposite signs, near the F_1/F_2 boundary where it vanishes. These peaks reflect the existence of a strong but short-ranged magnetic proximity effect. In F_2 and in F_1, τ_y is small and oscillatory. It reaches its maximum value at $\phi = 90^\circ$. It depends only weakly on the bias, since it basically reflects a static effect: the two magnets interacting with each other. This behavior is of course reflected in S_y as both quantities are related via Eq. (15).

The behavior of the in-plane components, x and z, is similar to each other (they are related by spin rotations) and quite different from that of y. Now currents and torques are transport-induced and one sees immediately that they markedly depend on bias. Since in F_1 the internal field always points along z, we find that S_z is a constant in F_1, its value increasing with bias. As a function of ϕ its behavior is complicated, the maximum value is not precisely at $\phi = 90^\circ$ and it is dependent on bias. For this value of ϕ the field points along the x direction in F_2 (it is always along z in F_1). Therefore S_z is always spatially constant in F_1 and this applies also to S_x in F_2 at $\phi = 90^\circ$. For other values of the mismatch angle S_x oscillates in both magnetic layers, and so does S_z in F_2. The amplitude of the oscillations of S_x decays slowly deep into the F_1 layer. In all cases the period of the spatial oscillations is approximately $1/h$ indicating that the oscillations are due to the behavior of the Cooper pairs. As to the corresponding components of the torque, one notes at once that their maximum value is much smaller than that of the τ_y peak but, away from the F_1/F_2 interface, the values are not all that different. This reflects the geometry, as explained above. We see that the x and z components of the torque are also nonmonotonic with ϕ, with peaks that are not necessarily at $\phi = 90^\circ$, depending on the bias. For lower biases, the peak values appear to shift away to smaller values, more closely aligned with the z direction, due to the increasing static effect from the F_1 layer. In our coordinate system, τ_z vanishes in F_1 for all ϕ and oscillates in F_2. Correspondingly, τ_x is oscillatory in both F_1 and F_2 except at $\phi = 90^\circ$ where it is zero in F_2. We have not plotted the magnetization itself, but its components exhibit damped oscillations which reflect the well known[51]precessional behavior of the magnetization around the internal fields. Such precessional behavior is then reflected in the current oscillations discussed above.

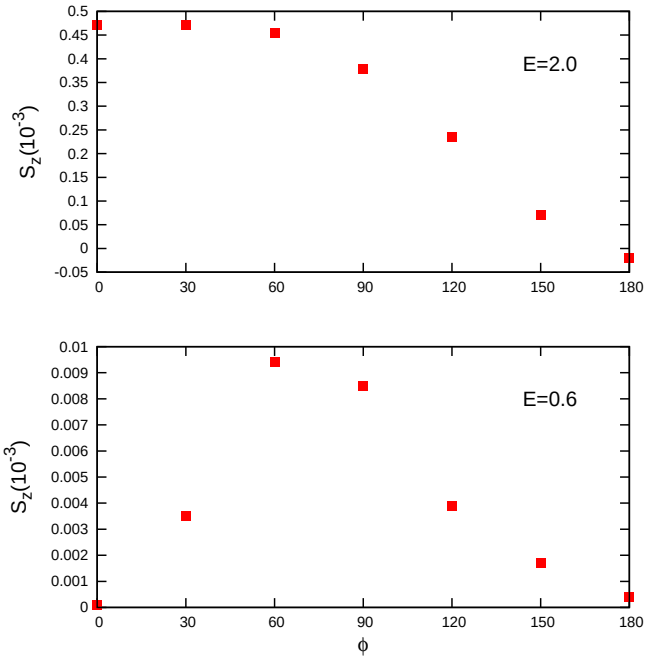

FIG. 10. The z component of the spin current in the outer F region as a function of ϕ, at two different bias values.

In our coordinate system, S_z is a constant in the outer layer, F_1. Also, all the components of the spin current are trivially constant in the S layer, since there are no torques there. As can be seen in Fig. 8, all spin current components vanish in S unless the bias exceeds the bulk S gap, Δ_0. This confirms the remarkable fact[8] that, in this respect, spin currents behave like charge currents in an N/S junction. It can rather easily be shown via standard spin rotation matrix arguments that the constant values of S_z and S_x deep in the S material, in the limit of large bias, should be approximately related to the value of S_z in the F_1 layer by factors of $\cos\phi$ and $\sin\phi$ respectively, and this can be seen in the last column of Fig. 8 to hold rather accurately at $E = 2$. On the other hand, the dependence of the constant value of S_z in the outer layer on ϕ is nontrivial as one can see in Fig. 8. We display this more clearly in Fig. 10, where we plot the value of S_z in F_1 at two different bias values. We see that for values below the CB the behavior is nonmonotonic: it cannot be, since S_z vanishes at both $\phi = 0$ and $\phi = 180^\circ$. The maximum value is near $\phi = 90^\circ$. On the other hand, when the bias is well above the CB, S_z, which in this case is non-vanishing at zero angular mismatch, decreases monotonically with ϕ. It becomes slightly negative when the two magnets are aligned in opposite direction. The behavior is not described by a simple trigonometric function and a simple argument leading to the behavior found seems elusive.

IV. CONCLUSIONS

The focus of this paper is on the prediction of the charge transport properties of superconducting spin valves with a $F_1/N/F_2/S$ layered structure. The emphasis is on studying systems having material and geometrical characteristics corresponding to samples that can realistically be experimentally fabricated. Our main results pertain to the conductance G as a function of bias, particularly with respect to the misalignment magnetization angle ϕ between the F layers: variation of this angle produces the desired spin valve effects. The conductance is the basic information which is experimentally obtained from charge transport measurements: it is the derivative of the current-voltage relation. To further our objective we have used values of the material parameters (such as the internal magnetic field and the superconducting coherence length) which have been previously shown[32] to fit with great accuracy the transition temperatures of such valve structures when the actual materials are Co, Cu and Nb. We have also used thickness values which encompass the available and desirable experimental ranges and have stayed away from idealistic assumptions, such as ideal interfaces, which are essentially irrelevant to actual experimental conditions. We have also studied the often neglected temperature dependence of the results. We have used a fully self consistent approach, which is absolutely necessary to ensure that charge conservation is satisfied.

Our results are summarized in Sect. III. The most important conclusion to be learned from the figures presented is that simple extrapolations are inadequate. There are several interfering oscillatory phenomena involved – the center of mass oscillation of the Cooper pairs in ferromagnets, the transmissions and reflections (ordinary, Andreev, and anomalous Andreev) at the three interfaces, and the usual quantum mechanical effects. As a result, the dependence of the relevant quantities that characterize the conductance (examples are the critical bias, the zero bias conductance, and the low and high bias features) have nonmonotonic behavior when just about any parameter in the problem varies. From this it follows that the valve effects, that is, the variation of G with ϕ, vary quantitatively and qualitatively depending on parameter values. The lack of monotonicity makes it extremely difficult to predict by extrapolation the measurable features expected for any given set of conditions. The only thing that makes sense is to build a database of conductance plots for different sets of parameter values, and compare the plots in the database with experimental results as they become available. We have built such a database–the results included here are a representative subset.

As far as the geometry dependence we have found that results depend most strongly on the thickness of the inner ferromagnetic layer, with a large dependence on the normal spacer thickness as well and a relatively weaker one on that of the outer F electrode. This is however an overall, general statement: specific details may be different. We have also found that the interfacial scattering specifically due to surface imperfections (the barriers), does not severely affect the valve effects for typical experimentally accessible values. Of course, scattering strong enough to destroy the proximity effect would be another matter. Another important conclusion we have reached is that temperature effects are not negligible in typical experimental situations. Furthermore, because of high derivative regions in the G vs. bias curves, a Sommerfeld expansion does not work well. However, an exact calculation can be performed numerically and it reveals that the shape of the conductance curve changes, becoming much smoother as bias varies, where as the valve effects as a function of ϕ remain unaffected.

We have also studied, in a much more limited way, the spin transfer torque and the spin currents in structures lacking the N layer. The results are analyzed in Sec. III D. We have found, in our geometry, that the y-component of the spin torques have sharp peaks at the F_1/F_2 interface, nearly independent of applied bias. These are due to the strong, static magnetic proximity effects. The greatest peak occurs for a mismatch angle ϕ of 90°. The spin torque components in the x and z direction are bias dependent and more complex, with higher peaks at angles smaller than $\phi = 90°$ for lower biases. We attribute this to static effects from the F_1 layer magnetization. We have calculated the spin currents using the direct method described in Eq. 14. We find a nonmonotonic behavior in the spin current amplitudes similar to that of the spin torque. The oscillation amplitudes tend to peak for angles slightly below $\phi = 90°$ for lower biases. The S_z component is constant in the F_1 layer and monotonic with angle for high bias values (above Δ_0) only. In the S layer, the spin currents are zero except for at high bias when both the S_x and S_z components attain nonzero values for most values of ϕ. The consistency between the torques and spin current gradients, imposed by the conservation laws, is ensured in our approach.

To conclude, the measurable quantities have complex behavior, often nonmonotonic as experimental parameters and inputs vary. Our plots provide an wide spectrum of features to study, many of which are not yet fully understood. We expect that the results we have obtained will provide a very important guide to experimentalists building real world superconducting spin valves in nanoscale heterostructures.

ACKNOWLEDGMENTS

The authors thank I.N. Krivorotov (University of California, Irvine) for many illuminating discussions on the experimental issues. They are very grateful to Chien-Te Wu (National Chiao Tung University) for many helpful discussions on all aspects of this problem. They also thank Yanjun Yang for technical help with the spin current calculations. This work was supported in part by DOE grant No. DE-SC0014467

* moenx359@umn.edu

† otvalls@umn.edu; Also at Minnesota Supercomputer Institute,

University of Minnesota, Minneapolis, Minnesota 55455
[1] E. Tsymbal and I. Žutić, *Handbook on spin transport and magnetism*, (CRC Press, Boca Raton, Florida 2012).
[2] A. Fert, Rev. Mod. Phys. 80, 1517 (2008).
[3] M. Eschrig, Rep. Prog. Phys. **78**, 104501 (2015).
[4] I. Žutić, J. Fabian, and S. Das Sarma, Rev. Mod. Phys.**76**, 323 (2004).
[5] Ya. V. Fominov, A.A. Golubov, T. Yu. Karminskaya, M. Yu. Kupryanov, R. G. Deminov, and L.R. Tagirov, JETP Lett. **91**, 308 (2010).
[6] A. I. Buzdin, Rev. Mod. Phys. **77**, 935 (2005).
[7] T. Yu. Karminskaya, A.A. Golubov, and M. Yu. Kupryanov, Phys. Rev. B**84**, 064531 (2011).
[8] C-T Wu, O.T. Valls and K. Halterman, Phys. Rev. B**90**, 054523, (2014).
[9] K. Halterman, O.T. Valls, and C-T Wu, Phys. Rev. B**92**, 174516 (2015).
[10] J. Zhu, I.N. Krivorotov, K. Halterman and O.T. Valls, Phys. Rev. Lett.**105**, 207002 (2010).
[11] E. A. Demler, G. B. Arnold, and M. R. Beasley, Phys. Rev. B**55**, 15174 (1997).
[12] Buzdin, A. I., and M. Y. Kuprianov, Pisma Zh. Eksp. Teor. Phys. **52**, 1089-1091 [JETP Lett. **52**, 487-491 (1990)].
[13] K. Halterman and O. T. Valls, Phys. Rev. B**65**, 014509 (2001).
[14] K. Halterman and O. T. Valls, Phys. Rev. B**66**, 224516 (2002).
[15] F.S. Bergeret, A.F Volkov, and K.B. Efetov, Phys. Rev. Lett.**86**, 3140 (2001); Phys. Rev. B**68**, 064513 (2003); Rev. Mod. Phys. **77**, 1321-1373 (2005).
[16] P.H. Barsic, O.T. Valls and K. Halterman, Phys. Rev. B**75**, 104502 (2007).
[17] K. Halterman and O. T. Valls, Phys. Rev. B**80**, 104502 (2009).
[18] V. L. Berezinskii, JETP Lett. **20**, 287 (1975).
[19] K. Halterman, P. Barsic and O.T. Valls, Phys. Rev. Lett.**99** 127002 (2007).
[20] F. Chiodi *et al.*, EPL **101**, 37002 (2012).
[21] C.T. Wu, O.T. Valls, and K. Halterman, Phys. Rev. Lett.**108**, 117005 (2012).
[22] C.T. Wu, O.T. Valls, and K. Halterman, Phys. Rev. B**86**, 184517 (2012).
[23] Y. Gu, G. B. Halász, J.W.A. Robinson, and M.G. Blamire, Phys. Rev. Lett.**115** 067201 (2015).
[24] F.S. Bergeret, A.F Volkov, and K.B. Efetov, Rev. Mod. Phys.**77**, 1321 (2005).
[25] M. Eschrig and T. Löfwander, Nature Physics **4**, 138 (2008).
[26] P.V. Leksin, N. N. Garif'yanov, I. A. Garifullin, Ya.V. Fominov, J. Schumann, Y. Krupskaya, V. Kataev, O. G. Schmidt, and B. Büchner, Phys. Rev. Lett.**109**, 057005 (2012).
[27] F. S. Bergeret, A. F. Volkov, and K. B. Efetov, Appl. Phys. A **89**, 599 (2007).
[28] Y. Kalcheim, O. Millo, A. DiBernardo, A. Pal and J.W. Robinson, Phys. Rev. B**92**, 060501 (2015).
[29] A. Singh, S. Voltan, K. Lahabi, and J. Aarts, Phys. Rev. X **5**, 021019 (2015).
[30] K.Halterman and M. Alidoust, arXiv:1607.03899 (2016)
[31] C.-T. Wu, O.T. Valls, and K. Halterman, Phys. Rev. B**86**, 014523 (2012).
[32] A. A. Jara, C. Safranski, I. N. Krivorotov, C.-T. Wu. A. N. Malmi-Kakkada, O. T. Valls, and K. Halterman, Phys. Rev. B**89**, 184502 (2014).
[33] A. F. Andreev, Sov. Phys. JETP **19**, 1228 (1964).
[34] J. Linder, T. Yokoyama, and A. Sudbø, Phys. Rev. B**79**, 224504 (2009).
[35] C. Visani, Z. Sefrioui, J. Tornos, C. Leon, J. Briatico, M. Bibes, A. Barthélémy, J. Santamaría, and Javier E. Villegas, Nature Phys. **8**, 539 (2012).
[36] Z. P. Niu, Europhys. Lett. **100** 17012 (2012).
[37] Y.-Q. Ji, Z.-P. Niu, C.-D. Feng, and D.-Y. Xing, Chinese Phys. Lett. **25**, 691 (2008)
[38] G. E. Blonder, M. Tinkham, and T. M. Klapwijk, Phys. Rev. B**25**, 4515 (1982).
[39] S. Kashiwaya, Y. Tanaka, M. Koyanagi, and K. Kajimura, Phys. Rev. B**53**, 2667 (1996).
[40] M. J. M. de Jong and C. W. J. Beenakker, Phys. Rev. Lett.**74**, 1657 (1995).
[41] I. Žutić and O. T. Valls, Phys. Rev. B**60**, 6320 (1999).
[42] I. Žutić and O. T. Valls, Phys. Rev. B**61**, 1555 (2000).
[43] P. G. de Gennes, *Superconductivity of Metals and Alloys* (Addison-Wesley, Reading, MA, 1989).
[44] Q. Cheng and B. Jin, Physica C: Superconductivity **473**, 29 (2012).
[45] P. H. Barsic and O. T. Valls Phys. Rev. B**79**, 014502 (2009).
[46] P.F. Bagwell, Phys. Rev. B**49**, 6841 (1993).
[47] F. Sols and J. Ferrer, Phys. Rev. B**49**, 15913 (1994).
[48] J. Sanchez-Canizares and F. Sols, Phys. Rev. B**55**, 531 (1997).
[49] G. Baym and L.P. Kadanoff, Phys. Rev. **124**, 287 (1961).
[50] N. W. Ashcroft and N.D. Mermin, *Solid State Physics*, (Philadelphia, PA 1976). See Appendix C.
[51] D.C. Ralph and M.D. Stiles, J. Magn, Magn. Mater. **320**, 1190 (2008).